Check for updates

Computer modeling of polymer stars in variable solvent conditions: a comparison of MD simulations, self-consistent field (SCF) modeling and novel hybrid Monte Carlo SCF approach

Alexander D. Kazakov, [ID] *[a] Varvara M. Prokacheva, [ID] [a] Filip Uhlík,[a]
Peter Košovan [ID] [a] and Frans A. M. Leermakers [ID] [b]

Computer-aided modeling is a systematic approach to grasp the physics of macromolecules, but it remains essential to know when to trust the results and when not. For a polymer star, we consider three approaches: (i) Molecular Dynamics (MD) simulations and implementing a coarse-grained model, (ii) the self-consistent field approach based on a mean-field approximation and implementing the lattice model due to Scheutjens and Fleer (SF-SCF) and (iii) novel hybrid Monte Carlo self-consistent field (MC-SCF) method, which combines a coarse-grained model driven by a Monte Carlo method and a mean-field representation driven by SF-SCF. We compare the performance of these approaches under a wide range of solvent qualities. The MD approach is formally the most exact but suffers from reasonable convergence. The mean-field approach works similarly in all solvent qualities but is quantitatively least accurate. The MC-SCF hybrid allows us to combine the benefits of the simulation route and the effective performance of SCF. We consider the center-to-end distance R_{ce}, the radius of gyration R_g^2 of the star and the polymer density profiles $\varphi(r)$ of polymer-segments in it. All three methods show a good qualitative agreement one to another. The MC-SCF method is in good agreement with the scaling predictions in the whole range of solvent quality values showing that it grasps the essential physics while remaining computationally in bounds.

1 Introduction

The polymer coil is one of the most soft objects known to man. Its softness, but also many other properties, continues to fascinate scientists across disciplines. There are various ways one can get deeper insight in its intricate behaviors. Computer aided modeling is a prominent tool that is frequently used for this. There are various methods all with their own pros and cons.

Computer simulations, for example, are used to predict effects such as the swelling or compression of coils, something that might be hard and/or expensive to lay your hand on using experiments. Simulations might also be used to deepen our knowledge in general.[1] With computer simulations, one typically samples phase space and by doing so one builds up knowledge of the (exact) system partition function. In turn, this function holds all insights that we can know about the system of interest. Their predictions are valuable and undeniably contribute to our knowledge. With the increasing strength of computer resources the computer simulation tool gains in importance.

In many cases, however, computer simulations do not (yet) resolve all issues. In particular, there may be length- and time scale challenges in combination with limited computational resources that prevent us from reaching acceptably small values for the statistical error estimation of targeted measurables. When this happens, one may even argue that it is meaningless to discuss values for the targeted effects, or one may even doubt whether simulations can relate to the existence *per se* of the targeted effect.

In cases when simulation methods are in trouble, that is in particular when satisfactory statistical accuracies cannot be reached, we may resort to alternatives. Invariably, these are based upon mean-field approximations and focus on the mean-field partition function. These approximations are implemented specifically to reduce the computation time and because in some cases, one can even make progress analytically. The mean-field approximation is a good example of sacrificing the system resolution to reach effective probability distributions.

[a] *Department of Physical and Macromolecular Chemistry, Faculty of Science, Charles University, Hlavova 8, 128 00 Praha 2, Czech Republic. E-mail: aleksandr.kazakov@natur.cuni.cz*

[b] *Department of Agrotechnology and Food Sciences, Wageningen University and Research Center, Wageningen, The Netherlands*

One prominent simulation method that gains importance, and is used below, is Molecular Dynamics (MD) simulations. MD samples the partition function by integrating the Newton law of motion. It accounts for correlations between segment interactions and therefore the method earned well-deserved recognition in the scientific audience and hence in the community of modeling of macromolecules. However, with an increasing number of segments in a polymer chain, MD simulation becomes less efficient and suffers from slow dynamics and accumulated errors.[2,3] For long polymer chains, we have to sacrifice the resolution of a system to get statistically reliable results. The MD technique is also limited because it has just one strategy to sample the degrees of freedom. When the dynamics is not *per se* of interest and the sampling of only the equilibrium properties is targeted, one can alternatively use the Monte Carlo (MC) simulation method. This method is an ensemble sampling approach that can make use of arbitrary changes of the system degrees of freedom and not necessarily ones that pass by through the motion of the molecule. By inventing arbitrary moves such that all phase space variables (typically the positional coordinates of all particles) can be reached, one can more effectively than MD, sample the Boltzmann distribution that characterizes equilibrium. MC can be used with exactly the same molecular model as MD and typically employs the Metropolis algorithm to guarantee that the Boltzmann distribution is indeed observed. When MD has trouble reaching the equilibrium distribution, also MC will quickly be in trouble. Hence the two methods are really complementary to each other but are limited in practice to 'small systems'.[2] MD may be preferred in cases when the coil is dense, while MC may be preferred for more open coils depending on the success of the sampling techniques. When the sampling is sufficiently rigorous both methods give the same exact results (for the same model).

The self-consistent field approach for inhomogeneous polymer systems using the Scheutjens–Fleer protocol (SF-SCF) is our mean-field approach that is embraced. This technique will not give the rigorous result, but an approximate one and also the model that is implemented has adjusted characteristics. In SF-SCF, one does not determine individual segment configurations, instead one evaluates their overall distributions based on the interactions of the segments with their averaged environment. This makes the method faster because, unlike in MD or MC, one averages over all chain configurations at once. This goes at the cost of neglecting some correlation and the method must of course be validated for each task that it is used for.

In this paper, we not only make use of the MD and the SF-SCF route, but specifically we elaborate on a hybrid method that combines the MC approach with the SF-SCF method such that we take advantage of the benefits of both methods. We will refer to this as the MC-SCF hybrid. In short, part of the degrees of freedom (segments) for the polymer coil will be managed by MC (so-called explicit segments). The remainder of the segments is handled by SF-SCF (so-called implicit segments). Importantly, the number of segments that is accounted for explicitly may be tuned and therefore we can go from a pure MC

model all the way to a pure SF-SCF model. While doing so we can handle some systems better than with the pure approaches. Meanwhile, we can keep the computational time within bounds.

The idea to use hybrid computational strategies is rather new and promising.[4–10] Ying Zhao *et al.* used the idea of a hybrid method to investigate the self-assembly in mixed solvents.[4] The authors mimic the micellization of Pluronic PEO$_{20}$–PPO$_{70}$–PEO$_{20}$(P123) in a water/ethanol/turpentine oil-mixed solvent by using the hybrid particle-field molecular dynamics (MD-SCF) method. Their simulation showed agreement with experiments with certain errors. Antonio De Nicola *et al.* were interested in the reproduction of micellar and non-micellar phases for Pluronic L62 and L64.[5] The authors reported that the reproduction of the studied morphologies depends on the concentration and temperature of these aqueous solutions. The modeling results with their hybrid method appeared in good agreement with the experimental phase diagrams. Johan Bergsma *et al.* simulated dendrimers in good solvent conditions.[6] These authors compared three models: a cell model (SF-SCF), the hybrid MC-SCF model and a freely-jointed chain model with excluded volume. They showed that the hybrid MC-SCF model gives a slightly different scaling and, unlike other models, also predicts a bimodal distribution for a large number of star arms and a multimodal distribution for dendrons of higher generations.

In all these works it was evident that hybrid methods go beyond the mean-field approximation because there is some account of correlations between segments. Meanwhile, of course, the speed of hybrid methods is not nearly that of the pure mean-field calculations which, compared to simulations, are ultra fast. Yet the method is often not as expensive as pure simulation approaches.

Our object of choice is the polymer star. One target of the current paper is to show that the MC-SCF hybrid, which can bridge between the pure MC and the pure SF-SCF, is able to give reliable results in all cases that we considered, whereas the pure MD has problems at long chain lengths and the pure 1-gradient SF-SCF suffers from the neglect of correlations.

We present the MC-SCF method and argue that the polymer star provides an excellent testing ground for it. We focus on the size and the radial density profile of such stars. The polymer star is the simplest example of branched polymers. Analytical predictions already exist for many of its properties. Also, these analytical predictions are put to the test. Hence there are interesting ways to check our results as well as test the predictions. We show that the MC-SCF method is a good alternative to pure MD simulations (equivalently to pure MC which we do not do) based on the coarse-grained (CG) model. The hybrid method produces good results in general. Needles to say, the MC-SCF method produces results that are superior to the 1D-SCF method.

The remainder of the paper is organized as follows. In the second section, we introduce the model for the polymer star that is considered and present the simulation protocols of each of the methods used. In the third section, we show how we have extracted various characteristics from the simulation data and

subsequently discuss the results. In the fourth section, we end with a summary of the results.

2 Models

In the present work, we compare different representation models of the polymer star. We use three models: coarse-grained (CG), mean-field (MF) and the hybrid of mean-field and coarse-grained representations; illustrations of these models are presented in Fig. 1. The polymer star consists of f arms (we limit to f = 3) with N segments per arm, the total number of segments could be counted as fN.

2.1 Coarse-grained model

In simulations, we embrace the coarse-grained (CG) model for computational reasons. Admittedly, in comparison to the all-atom models, the coarse-grained (CG) model has a relatively low resolution. Typically, in the CG model, one functional unit of a molecule is considered as one segment (bead). As usual, the solvent is represented as a structureless medium. This reduces the number of particles in the simulation box and additionally decreases the computational cost.

Despite such a coarse description, the model is widely used because of both qualitative and quantitative agreement with experiments.[11,12] Even with these approximations, it is unfortunate that one can simulate systems for only a limited range of time and length scales. To extend these limits even more, one should further reduce the resolution of the simulation but there is a limit to it. Eventually, one has to fall back onto mean-field models as explained above in a step-wise fashion. Below we will develop a hybrid method that allows us to fall back on the mean-field models in a systematic and gradual way.

All our MD simulations were performed using the *ESPResSo* package.[13] Both the non-bonded and bonded interactions are specified in these simulations. For the interactions between two non-bonding segments, we use the Lennard-Jones potential[14]

$$V_{\mathrm{LJ}}(r) = \begin{cases} 4\varepsilon\left[\left(\dfrac{\sigma}{r}\right)^{12} - \left(\dfrac{\sigma}{r}\right)^{6}\right], & \text{if } r < r_{\mathrm{cutoff}} \\ 0, & \text{elsewhere} \end{cases}, \qquad (1)$$
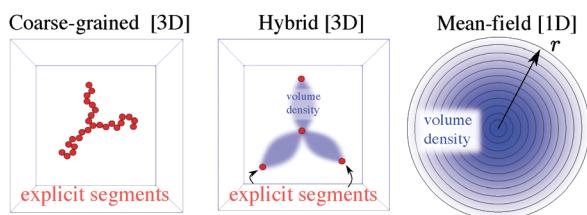

Fig. 1 Schematic representation of different models: (from left to right) the coarse-grained model in 3D, the hybrid model in 3D and the mean-field model in 1D. The coarse-grained model consists of explicit segments only (red beads). The hybrid model consists of both explicit segments (red beads) and implicit segments (blur). The mean-field model consists of implicit segments only (blur).

where r is the distance between the two segments in σ units, σ is treated as the size of the segments (at that point the potential is zero), ε is the depth of the potential well in $k_{\mathrm{B}}T$ units and r_{cutoff} is the cut-off distance beyond which the potential is zero, it has σ units. By varying either the depth ε and the cut-off r_{cutoff}, we tune the attractions between the segments. In a model with an implicit solvent, this means that these two parameters are used to tune the solvent quality of the polymers.

We use a finite extension nonlinear elastic (FENE) potential eqn (2) to account for the bonding interactions.[15] It is quite common to use a FENE potential for such a bead-spring polymer model because it accounts for nonlinear elastic extensions and as a consequence, the simulation is not constrained too much.

$$V_{\mathrm{FENE}}(r) = -\frac{1}{2}K\Delta r_{\max}{}^{2} \ln\left[1 - \left(\frac{r - r_0}{\Delta r_{\max}}\right)^{2}\right], \qquad (2)$$

where K is the magnitude of symmetric interaction between two segments, $\Delta r_{\max}$ is the maximal stretching length of the bond and r_0 is the equilibrium bond length. In our MD simulations we set $K = 10k_{\mathrm{B}}T/\sigma^2$, $\Delta r_{\max} = 2\sigma$ and $r_0 = 0$.[13]

We use the Langevin thermostat as implemented in the ESPResSo package. In the package, it is also necessary to specify the thermal energy $k_{\mathrm{B}}T$ and a constant that entails the coupling coefficient with the bath γ. We set the following parameters: $k_{\mathrm{B}}T = 1.0$ and $\gamma = 1.0$.[13]

2.2 Mean-field model

The mean-field (MF) model implements another strategy to reduce the studied system resolution. The idea behind it is to approximate particle–particle interactions by interactions with a density field. It provides an opportunity to simulate systems of bigger sizes without an unacceptable increase in computational costs. Typically, such models are lattice based.

The classical example of a MF model is the Flory–Huggins (FH) theory. In FH theory it is assumed that no (polymer) density variations exist throughout the system. In the present work, we use the Scheutjens-Fleer self-consistent field method, which exploits ideas from the Flory–Huggins theory, yet taking density variations (typically in one direction, but higher dimensions are also elaborated) into account.[16,17] It is based on an approximation of explicit pairwise interactions between particles by interactions that are proportional to the average local density of the interacting species. As already mentioned this approximation reduces the computational costs dramatically. At the same time, the MF approach is a reliable alternative to full-scale simulations in terms of accuracy.[18]

The mean-field approximation works well when correlations between individual particles are not too strong. In such a case, it is well justified to replace the explicit particle–particle interactions with the average probability of the interaction defined by the density. In the case of strong correlations, the mean-field approximation fails and an explicit particle representation is required.
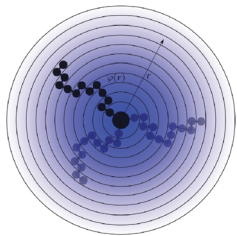
Fig. 2 Schematic representation of 3-arm star in mean-field model in 1D-SCF.

We use the one-gradient Scheutjens–Fleer self-consistent field (1D-SCF) approach to model the polymer star in the mean-field approximation. The classical Scheutjens-Fleer theory is well described in literature.[6,10,16,19–21] Here we outline the ideas in the context of the modeling of a polymer star.

The one-gradient SF-SCF method for a polymer star takes the center of the star at the center of a spherical coordinate system. In a star with f equivalent arms, we can make optimal use of the symmetry and evaluate the segment distribution for just one arm and multiply the result by f, see Fig. 2. This trick reduces the computational time dramatically. In order to allow a detailed description of how the SF-SCF protocol is implemented in the hybrid method, it is necessary to go into slightly more detail.

The SF-SCF approach is constructed around a mean-field Helmholtz energy functional, which features the density profiles (both for the solvent and the polymer) the corresponding potential profiles and Lagrange parameters that take care of the incompressibility constraint.[10,22–24] The saddle point of this free energy leads to the SF-SCF rule on how to compute the volume fraction (densities) from potentials and another rule on how to compute the potentials from the volume fractions. We need to implement these rules both for the monomeric solvent and for the polymer segments in the star. The Lagrange parameters must be chosen such that the considered solution obeys the incompressibility condition: $\sum_j \varphi_j(\vec{r}) = 1$, where the sum goes through all types of polymer segments and monomeric solvent.

The volume fraction profile of the solvent $\varphi_s(\vec{r})$ is coupled to the corresponding potential profile $u_s(\vec{r})$ through Boltzmanns law:

$$\varphi_s(\vec{r}) = C_s \exp(-u_s(\vec{r})), \tag{3}$$

where it is understood that the potentials are already normalized by $k_B T$ and C_s is a constant determined from the normalization. In the case that far from the star there is only the solvent, we can set $C_s = 1$. The potentials that feature in the Boltzmann weight are coupled to the volume fractions of the polymer $\varphi(\vec{r})$ (how the polymer density is computed is discussed below)

$$u_s(\vec{r}) = \alpha(\vec{r}) + \chi(\langle\varphi(\vec{r})\rangle - \varphi^b), \tag{4}$$

where χ is the dimensionless Flory–Huggins parameter, and $\alpha(\vec{r})$ is the Lagrange multiplier. The bulk volume fraction of polymer φ^b is introduced to ensure that the potentials are zero in the bulk, but because the bulk concentration is zero for a pinned star,

we may also leave this quantity out in this case. The angular brackets implement a three-layer average. This local averaging is a hall-mark of the Scheutjens-Fleer approach. Especially when the χ-parameter is high and large gradients in density exist, it is necessary to account for these gradients. The three-layer average is computed by

$$\langle\varphi(\vec{r})\rangle = \lambda(\vec{r}, \vec{r}-1)\varphi(\vec{r}-1) + \lambda(\vec{r}, \vec{r})\varphi(\vec{r}) + \lambda(\vec{r}, \vec{r}+1)\varphi(\vec{r}+1) \tag{5}$$

for each $\vec{r}$ the three transition probabilities obey to

$$\lambda(\vec{r}, \vec{r}-1) + \lambda(\vec{r}, \vec{r}) + \lambda(\vec{r}, \vec{r}+1) = 1.$$

We choose

$$\lambda(\vec{r}, \vec{r}-1) = \frac{1}{6}\frac{A(\vec{r}-1)}{L(\vec{r})}; \quad \lambda(\vec{r}, \vec{r}+1) = \frac{1}{6}\frac{A(\vec{r})}{L(\vec{r})},$$

where $A(\vec{r}) = 4\pi r^2$ and $L(\vec{r}) = V(\vec{r}) - V(\vec{r}-1)$ with $V(\vec{r}) = \frac{4}{3}\pi r^3$. With this strategy it can be shown that $\langle\varphi(\vec{r})\rangle \approx \varphi(\vec{r}) + \frac{1}{6}\nabla^2\varphi(\vec{r})$ in the continuous limit.

The evaluation of the polymer segment distribution is slightly more involved and requires a choice for the chain model. A popular chain model that is often implemented is the lattice variant of the freely jointed chain model. Within this model, there is a simple propagator formalism to find the polymer volume fractions. In this propagator formalism two complementary end-point distributions appear: $G(\vec{r}', s'|1, 1)$ and $G(\vec{r}', s|N)$. The first one contains the statistical weight for all walks that start with segment $s = 1$ at coordinate $\vec{r} = 1$ (center of the coordinate system) and ends at segment $s = s'$ at coordinate $\vec{r} = \vec{r}'$. The second one contains the combined statistical weight for all walks that started with $s = N$ (the free end) at any location and ends at the same coordinate $\vec{r} = \vec{r}'$ with segment $s = s'$. The volume fractions are given by the combination of these two end-point distributions. This combination is usually referred to as the composition law:

$$\varphi(\vec{r}) = \sum_{s=1}^{N} C\frac{G(\vec{r}, s|1, 1)G(\vec{r}, s|N)}{G_1(\vec{r})}, \tag{6}$$

where C is a normalisation constant such that $fN = \sum_{\vec{r}} L(\vec{r})\varphi(\vec{r})$. The normalization by the free segment distribution $G_1(\vec{r}) = \exp(-u(\vec{r}))$ is needed to prevent double counting for the statistical weight of the overlapping segment s. The two end-point probability functions are found by the following recurrence relations:

$$G(\vec{r}, s|1, 1) = \langle G(\vec{r}, s-1|1, 1)\rangle G_1(\vec{r}) \tag{7}$$

$$G(\vec{r}', s|N) = \langle G(\vec{r}', s+1|N)\rangle G_1(\vec{r}) \tag{8}$$

also known as the forward and backward propagators, respectively. Both propagators need suitable initiations. For the forward propagator we need to account for the fact that the chain starts at the center of the spherical coordinate system and therefore $G(\vec{r}, 1|1, 1) = G_1(\vec{r})\delta(\vec{r}, 1)$, where $\delta(\vec{r}, 1) = 1$ when

$\vec{r} = 1$ and zero otherwise. The backward propagator is initiated without constraints, that is $G(\vec{r}, N|N) = G_1(\vec{r})$.

Finally, we need the segment potentials; these are a function of the volume fractions of the solvent:

$$u(\vec{r}) = \alpha(\vec{r}) + \chi\left(\langle\varphi_s(\vec{r})\rangle - \varphi_s^b\right). \tag{9}$$

As $\varphi_s^b = 1$ (outside the star, that is in the bulk, there is only the solvent) and again the potentials are set to zero at large values of $\vec{r}$ (far from the star).

The above set of equations, in general, cannot be solved analytically: we need the segments and solvent volume fractions to compute the potentials and *vice versa*. Also, we need values of the Lagrange parameters α. A fixed point of these equations is routinely found numerically using an iterative method. In the absence of a suitable initial guess, one typically starts with zeros for both the Lagrange parameters and the potentials. Then the segment and solvent densities can be computed. The Lagrange parameters are updated $\alpha^{new}(\vec{r}) = \alpha^{old}(\vec{r}) + \beta(\varphi(\vec{r}) + \varphi_s(\vec{r}) - 1)$ with a suitable parameter $0 < \beta < 1$. Next, the potentials $u(\vec{r})$ may be recomputed and updated: $u^{new}(\vec{r}) = (1 - \beta)u^{old}(\vec{r}) + \beta u(\vec{r})$ (for both the polymer segments and the solvent). This procedure can be repeated until convergence is reached. Typically, however, such a scheme is slow and in practice a more sophisticated algorithm is used, which reaches convergence in order 100 iterations and then at least 7 significant digits is reached.[25]

Once the SCF fixed point is found, we know not only the density distributions, but we can also evaluate the (mean-field) Helmholtz energy F of the system. The latter one (in units of $k_B T$) is given by

$$F = -\ln Q - \sum_{\vec{r}}(u(\vec{r})\varphi(\vec{r}) - u_s(\vec{r})\varphi_s(\vec{r}))$$
$$+ \sum_{\vec{r}} L(\vec{r})\chi\varphi_s(\vec{r})\langle\varphi(\vec{r})\rangle, \tag{10}$$

where the system partition function Q may be decomposed into molecular partition functions, $Q = q\dfrac{q_s^{n_s}}{n_s!}$, wherein the solvent partition function $q_s = \sum_{\vec{r}} L(\vec{r})\exp(-u_s(\vec{r}))$ and the polymer partition function $q = (L(1)G(1,1/N))^f$. The number of solvent molecules, n_s, is given by $n_s = \sum_{\vec{r}} L(\vec{r})\varphi_s(\vec{r})$.

2.3 Hybrid model

The hybrid MC-SCF method is based on a combination of the mean-field and the coarse-grained models. Instead of MD, we use the MC solver for the coarse-grained model. It represents selected segments of the system as explicit particles, and the remaining (implicit) segments as a density field, shown in Fig. 1. All work now is done in a 3-dimensional box of lattice sites, each coordinate x–y–z has M lattice sites, where M is large enough so that the system boundaries do not affect the conformational properties of the central star.

Idea of MC-SCF fragments. With a protocol discussed below the star, the molecule is split into a number of fragments, which we may number $k = 1, \ldots, K$. Each of these fragments has a

length n segments and is bracketed by explicit segments. The task for SF-SCF is to compute for each of these fragments the Helmholtz energy F_k (as well as the distributions of the segments). For this, we slightly deviate from the above SF-SCF protocol. Instead of a one-gradient approach, we now have to consider three gradients. The first and last coordinates (explicit segments) of a given fragment number k are given by $\vec{r}_k^0$ and $\vec{r}_k^{n+1}$, respectively. These coordinates are provided by the MC protocol. We design a sub-box around these two points so that with SF-SCF we can efficiently compute the Helmholtz energy for this sub-box. The size of the sub-box is $m \times m \times m$ lattice sites, where we notice that frequently m may be significantly smaller than M. The position of the boundaries of the sub-boxes k is ideally far away from the coordinates of the two explicit segments so that the fragment in between the constraining segment can not reach the sub-box boundary. Nevertheless, at the boundaries of the sub-boxes, we implement reflecting (mirror-like) boundary conditions so that in cases that the sub-walks hit the sub-box boundaries the adverse effects are minimized.

The MC-SCF hybrid is rather flexible in how the workflow is distributed between the MC and the SCF parts. When computational efficiency is important one typically should aim for long fragments n and thus few MC-degrees of freedom (relatively few explicit segments). In this case, the MC-sampling is less demanding and this outweighs the increase in workload for the SCF part. Inversely when the 'correctness' of results is most evident, one should strive for more MC particles (explicit segments) and thus shorter fragments. The more explicit segments in the model the higher is the potential to account for the excluded volume effects.

SCF procedure in the MC-SCF method. We have to extend the above protocol so that the SCF equations take three spatial coordinates $(\vec{r} = (x, y, z))$ into account. So both the potentials and the densities are now needed for all spatial coordinates. Now $L(\vec{r}) = 1$ for all coordinates. Let us assume that for the sub-box k we know the potentials for all its coordinates. The evaluation of the polymer volume fractions for fragment k requires the use of the composition law, which now features two end-point distributions $G_k(\vec{r}, s|\vec{r}_k^0, 0)$ and $G_k(\vec{r}, s|\vec{r}_k^{n+1}, n+1)$, as both the begin as well as the end of the walk of the fragment is specified:

$$\varphi_k(\vec{r}) = \sum_{s=1}^{n} C\frac{G_k(\vec{r}, s|\vec{r}_k^0, 0)G_k(\vec{r}, s|\vec{r}_k^{n+1}, n+1)}{G_1(\vec{r})}, \tag{11}$$

where again C is computed such that $n = \sum_{\vec{r}} \varphi_k(\vec{r})$. The propagators can be initiated by $G_k(\vec{r}, 0|\vec{r}_k^0, 0) = 1$ for $\vec{r} = \vec{r}_k^0$ and zero otherwise, and similarly, $G_k(\vec{r}, n+1|\vec{r}_k^{n+1}, n+1) = 1$ when $\vec{r} = \vec{r}_k^{n+1}$ and zero otherwise. The propagators now read

$$G_k(\vec{r}, s|\vec{r}_k, 0) = \langle G_k(\vec{r}, s-1|\vec{r}_k, 0)\rangle G_1(\vec{r}) \tag{12}$$

$$G_k(\vec{r}, s|\vec{r}_k, n+1) = \langle G_k(\vec{r}, s+1|\vec{r}_k, n+1)\rangle G_1(\vec{r}). \tag{13}$$

In the three-gradient system, the angle brackets are computed as

$$\langle G(x,y,z)\rangle = \frac{1}{6}(G(x-1,y,z) + G(x+1,y,z) + G(x,y-1,z)$$
$$+ G(x,y+1,z) + G(x,y,z-1) + G(x,y,z+)) \quad (14)$$

The overall volume fraction of the segments that are accounted for by SCF is found by a summation over all the sub-boxes:

$$\varphi(\vec{r}) = \sum_k \varphi_k(\vec{r}). \quad (15)$$

The corresponding potentials are found by eqn (9) implemented for the x–y-z coordinates and with the proper definition of the angle brackets. The evaluation of the solvent density and potentials are computed likewise.

With this revised protocol it is possible to find again the SF-SCF fixed point. The overall Helmholtz energy (a 3-gradient variant of the Helmholtz energy is obtained similarly as in eqn (10) with straightforward minor adjustments) for the overall system is found by the summation over the SF-SCF Helmholtz energies per sub-box, that is $F = \sum_k F_k$. This overall Helmholtz energy is to be used in the MC protocol.

MC procedure in the MC-SCF method. There are a few salient features that we need to mention at this stage. Typically, the explicit segments are assumed to have a density of unit at the specified coordinates and therefore the implicit segments cannot enter the site already taken by the explicit segments. This is implemented by putting the statistical weight G_1 to zero for these 'taken' sites. When the sub-boxes overlap it can happen that in the sub-box explicit segments occur that are linked to other fragments. Then also for these taken sites the statistical weights G_1 are set to zero. Hence, all coordinates that are occupied by explicit segments were excluded for the implicit ones. Secondly, by virtue of the cubic lattice, starting and finishing positions for a fragment with length n are allowed. There is an even/odd problem, but this problem is trivially accounted for in the MC protocol that generates the starting and stopping coordinates for each fragment k.

The task for the MC protocol is to find successive explicit particle positions in order to sample the positional degree of freedom of the star segments. The movement is driven by Monte Carlo (MC) protocol. We implemented Metropolis–Hastings algorithm with nested Monte Carlo cycle with an approximate inner potential within.[26] In the inner loop the acceptance criterion for the MC trial moves is the standard Metropolis criterion,[27] but instead of the internal energy of the system, the criterion uses the potentials of mean force (as computed by a Helmholtz energy equivalent to eqn (10), but of course computed for the model used in the hybrid strategy as already mentioned) F, as an input.

The probability of acceptance for MC moves is the following:

$$p = \min\big(1, \exp\{-\beta[F^{\text{new}}(\vec{r}') - F^{\text{old}}(\vec{r})]\}\big), \quad (16)$$

where F^{new} and F^{old} are the potentials of mean force with the explicit segments placed at coordinates $\vec{r}'$ in the old configuration and at $\vec{r}$ in the new configuration, respectively.

In the outer loop we use Metropolis–Hastings acceptance criterion:

$$p = \min\left(1, \frac{\pi_j \pi_i'}{\pi_i \pi_j'}\right), \quad (17)$$

where π_j and π_i are trial and current configurations, respectively, calculating by the SCF part of the MC-SCF method. The π_j' and π_i' are trial and current configurations calculating (in the inner loop) by following approximate potential:

$$F_k = \frac{3}{2}\frac{R_k^2}{N}$$
$$+ V_k\left(\left(1 - \frac{N}{V_k}\right)\ln\left(1 - \frac{N}{V_k}\right) + \chi\frac{N}{V_k}\left(1 - \frac{N}{V_k}\right)\right), \quad (18)$$

where $V_k = R_k^3 N^{3\nu}$, for all solvent quality conditions $\nu = 0.9$. The approximate potential consists of 3 terms: conformational, translational entropy of solvent, and interactions term.

To summarize the above hybrid protocol we can say that the potentials of mean force correspond to the Helmholtz energies obtained from the SF-SCF calculation keeping the explicit segments fixed at given positions and averaging over all possible locations of the remaining implicit segments.[6,22] In this way, we can account for local density fluctuations on the level of explicit segments, beyond the mean-field level, and simultaneously reduce the computational cost as compared to explicit particle simulations.

MC trials. We have implemented three types of MC-moves: pivot, "one-bond", and one-node movements. We randomly choose a type of movement on each MC step. By this, we try to sample configurational space as fast as possible.

The idea of the pivot movement is shown in Fig. 3. Firstly, we randomly choose the explicit node in one of the star arms (the empty segment in Fig. 3). After that, starting from the chosen node and further to the end of the star arm, we rotate all nodes as one rigid object with an angle θ. The angle of rotation due to simple cubic geometry could be only $\pm\pi/2$.

The "one-bond" movement is another type of movement in our implementation. This type of movement is needed because the pivot movements cannot reach all degrees of freedom. The one-bond movements fill in for these missed positional degrees of freedom. By this movement only one "bond" in the system changes, by "bond" now we mean implicit segments between two neighboring nodes. We choose randomly one node and therefore we split the star into 2 sets of nodes. The first set is all
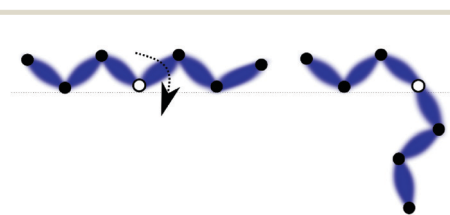

Fig. 3 The idea of the pivot movement. Circles represent nodes, blue connections are implicit polymer segments.

nodes excluded the chosen node and nodes, which go after the chosen one. The second set of nodes is the total number of nodes minus the first set. By using these two sets we can move only one "bond" of the star. This means that all nodes in one of the sets are shifted by the same amount.

The one-node move is the simplest movement in the MC-SCF method. By this movement only one randomly picked node is moved by one lattice point.

Using these three types of movements we successfully sample polymer star at any solvent quality conditions using the MC-SCF method.

2.4 Simulation protocols

We perform simulations for a number of solvent qualities for one polymer star with $f = 3$ arms and a different number of segments per arm N in a range from $N = 20$ up to $N = 200$.

We choose appropriate box sizes for each of the methods. The box size at least must fit the star and should exceed $N^{0.6}$. In principle, the upper limit is not restricted. Simulation boxes for the MD and the MC-SCF methods were identical. The performance of an MD simulation strongly depends on the number of beads (segments) and not on the box size. In the MC-SCF method, the performance does depend on the size of the box size. More accurately, it depends on the sizes of the MC-SCF fragment (sub-box) and the number of fragments in the star. Taking this into account, we varied box size from $box_l = 32$ for $N = 20$ up to $box_l = 90$ for $N = 200$. In the 1D-SCF method, the simulation box was chosen in order to satisfy $box_l = N[\text{units}] + 5$ so that none of the segments of the star can reach the system boundary.

For the MD method we equilibrated all systems within 12 hours, after that we run production simulation for 24 hours. For the MC-SCF method we run simulation only for 24 hours. All methods we simulated on similar, in terms of efficiency, CPU cores. For comparison reasons, we used only one CPU core from one processor per simulation. For small systems ($N \leq 60$) this condition was more than sufficient to reach good statistical accuracies. For the 1D-SCF method, all these restrictions are irrelevant because the calculation of any of the systems took less than 1 CPU minute.

2.4.1 MD method. The simulation protocol for the MD method is straightforward. We construct an initial configuration of the star. After construction, we turn on the bonded and non-bonded interactions between all segments. After that, we do a sufficiently long equilibration run. Finally, we let the system evolve while data is collected.

2.4.2 1D-SCF method. In order to simulate polymer star using the 1D-SCF method, we apply spherical symmetry. We consider only one linear chain fixed to the center of the simulation box with a certain volume density, which corresponds to the defined number of the arms Fig. 2. After SF-SCF minimization, we have a polymer star in an equilibrium state for a specified value of the χ parameter.

2.4.3 MC-SCF method. A simulation protocol for the MC-SCF method can be summarized as follows:

1. construct the initial configuration of the system;

2. calculate the free energy of the system F^{old} using the SCF part of the MC-SCF method and approximate potential eqn (18);

inner loop:

(a) for each inner step (we do 3 times) do following:

(b) choose an explicit segment;

(c) choose a type of movement (pivot, 'one-bond' or one-node);

(d) move corresponding (to movement) explicit segments;

(e) calculate the free energy of the system F^{new} using eqn (18);

(f) accept with probability P (see eqn (16)) and update the positions of explicit segments. When the new positions are rejected, return all explicit segments to the old positions;

3. calculate the free energy of the system F^{new} using SCF part of the MC-SCF method and approximate potential eqn (18);

4. accept with probability P (see eqn (17)) and update the position of explicit segments. When the new positions are rejected, return all explicit segments to old positions;

5. go to inner loop.

We emphasize that the MC-SCF method distinguishes all explicit segments of the star. By choosing one explicit segment we choose (in pivot move) only one arm of the star.

3 Results and discussion

3.1 Data analysis

In order to compare different models, we use the center-to-end distance R_{ce}, the radius of gyration R_{g}^2 of the star and its radial volume fraction distribution $\varphi(r)$.

Let us start with the center-to-end distance R_{ce}. Due to the fact that the star has several arms, we should take an average of distances from the center to the end of each arm:

$$R_{\text{ce}} = \frac{1}{f} \sum_{i=1}^{f} r_{\text{center-to-end}, i}, \tag{19}$$

where f is the number of arms, $r_{\text{center-to-end}, i}$ is the distance from the center of the star to the end of the arm number i. eqn (19) can be applied to both CG and hybrid models because in CG the positions of all segments at any time are available and in the hybrid method the ends are also available. In the 1D-SCF method, instead of all positions of all segments, we have a distribution of the ends of the star. That is why eqn (19) is not used. A typical end-point distribution is presented in Fig. 4. Using this distribution we calculate the average distance of the ends from the center with eqn (20):

$$R_{\text{ce}} = \sum_{\vec{r}} \frac{r \varphi_{\text{ends}}(\vec{r}) L(\vec{r})}{\varphi_{\text{ends}}(\vec{r}) L(\vec{r})}, \tag{20}$$

where r is a distance from the center to a layer in spherical geometry, $\varphi_{\text{ends}}(\vec{r})$ is the volume density of the ends of the star in $\vec{r}$, $L(\vec{r})$ is the number of cells in $\vec{r}$, sum goes from the first layer to the end of the simulation box.
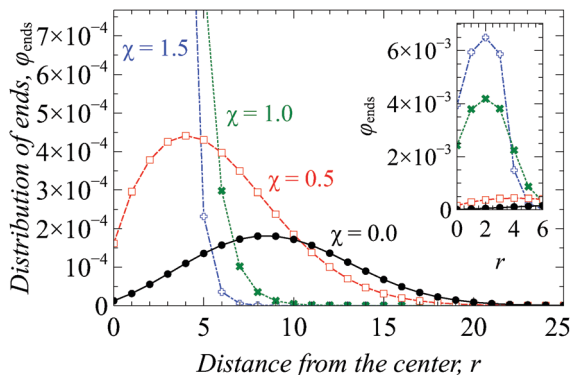
Fig. 4 1D-SCF method. The distribution of the ends of the star consisted of $f = 3$ arms with length $N = 100$ monomers. Different colors correspond to different solvent quality χ.

The radius of gyration R_g^2 for branched polymers is defined as:

$$R_\mathrm{g}^2 = \frac{m_\mathrm{seg}}{M_\mathrm{tot}} \sum_i (\vec{r}_i - \vec{r}_\mathrm{cm})^2, \qquad (21)$$

where $(\vec{r}_i - \vec{r}_\mathrm{cm})^2$ is a distance between monomers at a given coordinate (position vector $\vec{r}_i$) and the polymer center of mass (position vector $\vec{r}_\mathrm{cm}$), m_seg is the mass of the segment, M_tot is the total mass of the polymer. The sum goes over all segments.

The vector to the center of mass is given by:

$$\vec{r}_\mathrm{cm} = \frac{m_\mathrm{seg}}{M_\mathrm{tot}} \sum_i \vec{r}_i. \qquad (22)$$

All simulations are constructed in a way that the center of the polymer star is fixed in the center of the simulation box. At the same time for the CG model, all segments have the same mass $m_\mathrm{seg} = 1$. eqn (21) and (22) need slight modifications for the hybrid and mean-field models.

In the MC-SCF method, we apply the following equation for the radius of gyration:

$$R_\mathrm{g}^2 = \frac{\sum_{\vec{r}} \varphi(\vec{r})(\vec{r} - \vec{r}_\mathrm{cm})^2}{\sum_{\vec{r}} \varphi(\vec{r})}, \qquad (23)$$

where $\varphi(\vec{r})$ is the volume fraction of the star at $\vec{r}$, $(\vec{r} - \vec{r}_\mathrm{cm})^2$ is the distance between a monomer in $\vec{r}$ and the polymer's center of mass. The sum runs over all vectors $\vec{r}$.

To calculate the center of mass we use:

$$\vec{r}_\mathrm{cm} = \frac{\sum_{\vec{r}} \vec{r}\varphi(\vec{r})}{\sum_{\vec{r}} \varphi(\vec{r})}. \qquad (24)$$

In the 1D-SCF method, we computed the radius of gyration with:

$$R_\mathrm{g}^2 = \frac{\sum_{\vec{r}} \vec{r}^2 \varphi(\vec{r}) L(\vec{r})}{\sum_{\vec{r}} \varphi(\vec{r}) L(\vec{r})}, \qquad (25)$$

where $\vec{r}^2$ is the distance in lattice units to the center of the coordinate system (here, it is in the center of the simulation box), $\varphi(\vec{r})$ is a volume density of the star in coordinate $\vec{r}$, $L(\vec{r})$ is a number of cells in $\vec{r}$. The sum runs again from the first layer to the end of the simulation box.

Different solvent quality conditions are reached differently in different methods. In the MD case, the interactions between the monomers are defined by the Lennard-Jones potential. However, in 1D-SCF and MC-SCF methods, the Flory–Huggins parameter χ is used.

Good solvent quality condition in the CG model can be reached by tuning ε and r_cutoff parameters in eqn (1). Particularly, we choose $\varepsilon = \sigma = 1$, $r_\mathrm{cutoff} = 2^{1/6}\sigma$, where σ is size of the particles. By setting such values to the Lennard-Jones potential we convert the potential to the Weeks–Chandler–Anderson (WCA) potential, which represents only the repulsive part of the interaction curve.[28] However, by proper settings of ε and σ as well as r_cutoff we can work in Θ and poor solvent quality conditions.

To apply a Θ-solvent condition in the MD method is not trivial. Indeed, it is not easy to map the Lennard-Jones parameters to get truly accurate values of ε and r_cutoff.[29] We consider to be close to the Θ-solvent quality for the following setting: $\varepsilon = 0.34$, $r_\mathrm{cutoff} = 2.5\sigma$, where $\sigma = 1.0$.

In order to simulate poor solvent conditions in the MD method, we fixed $r_\mathrm{cutoff} = 2.5\sigma$ and $\varepsilon = 0.7$. At such parameters, additionally, to repulsive part of the potential, we have an attractive part.

Any solvent quality conditions in 1D-SCF and MC-SCF methods are controlled by the Flory–Huggins parameter χ. In these terms, $\chi = 0.0$ refers to good solvent, $\chi = 0.5$ refers to Θ-solvent, and $\chi > 0.5$ corresponds to a poor solvent quality condition. We have used $\chi = 0.0$, 0.5, and 1.5 to go from good, via Θ to poor solvent quality.

In order to estimate error bars of the properties of the system, for each property, the autocorrelation function was computed. With this function, we can estimate how many uncorrelated (independent) samples we have overall. Thus, we can estimate the standard error of the mean by:

$$\sigma_\mathrm{err} = \frac{s}{\sqrt{n}},$$

where s is the sample standard deviation, n is a number of independent samples.

3.2 Center-to-end distance, R_ce

We performed several sets of simulations of one star in a box at different solvent quality conditions: good solvent quality, where the repulsion between segments of polymer star is dominant, poor solvent, where attractive interactions between segments are dominant, and Θ-solvent, where the probability of pair collisions is zero.

Following the scaling theory,[30,31] we plot several master curves for checking the results from simulations. The scaling theory predicts dependency of $R_\mathrm{ce} \propto N^\gamma$, where N is the number
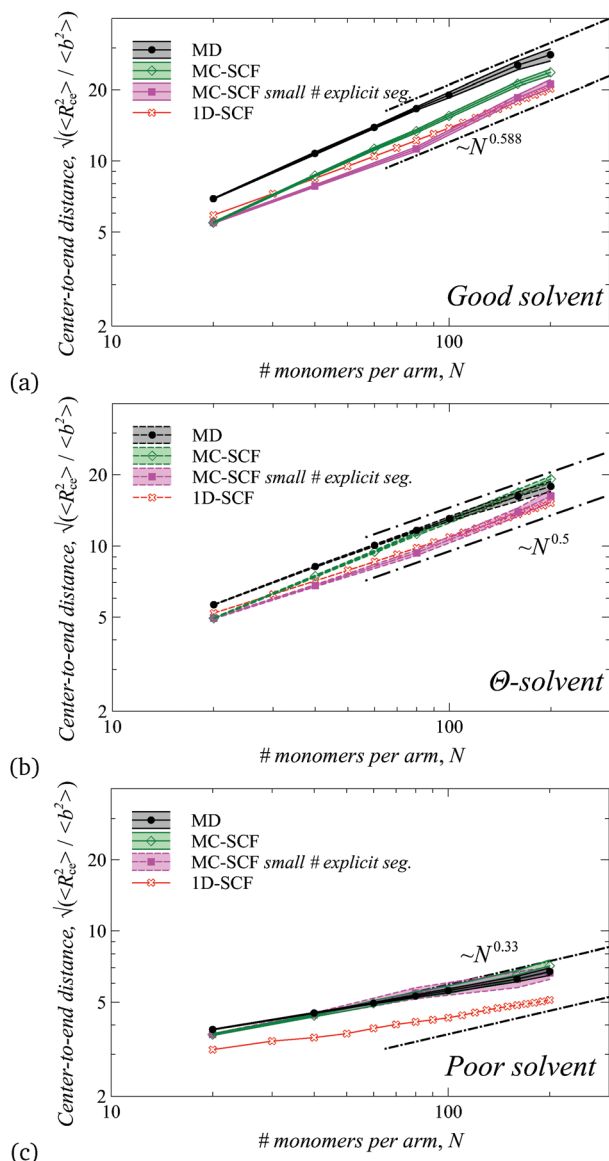
Fig. 5 $\sqrt{\langle R_{ce}^2\rangle/\langle b^2\rangle}$ of the star for MD, MC-SCF and 1D-SCF methods, where $\beta\langle b^2\rangle$ is averaged bond length in MD and $\langle b^2\rangle = 1$ for MC-SCF and 1D-SCF. Figure (a) represents data from simulations in a good solvent: MD parameters $\varepsilon = 1.0$, $r_{cutoff} = 2^{1/6}$, MC-SCF and 1D-SCF parameter $\chi = 0.0$. Figure (b) corresponds to Θ-solvent: MD parameters $\varepsilon = 0.34$, $r_{cutoff} = 2.5$, MC-SCF and 1D-SCF parameter $\chi = 0.5$. Figure (c) Poor solvent quality conditions: MD parameters $\varepsilon = 0.7$, $r_{cutoff} = 2.5$, MC-SCF and 1D-SCF parameter $\chi = 1.5$. The number of explicit segments in the MC-SCF method (green curve) could be calculated by $(fN/n) + 1$, where $f = 3$, $n = 20$. In MC-SCF with a small number of explicit segments (pink curve), the number of explicit segments equals 4 in the region $N \leq 80$, elsewhere 7. The shaded area represents the estimated error for the value.

of segments in an arm, γ is a power which goes from $\gamma = 0.33$ for poor solvent to $\gamma = 0.588$ for good solvent.

In Fig. 5 dependencies of center-to-end distance R_{ce} are shown as a function of the number of segments N in the arm of the star in different solvent quality conditions.

In Fig. 5a the dependency R_{ce} is shown at good solvent quality conditions. In agreement with scaling predictions,

all curves obey the scaling law for good solvent condition $\gamma \approx 0.588$. The 1D-SCF is the fastest method and gives the smallest values for R_{ce} for all lengths of star arms. Indeed, as it could be expected the MC-SCF method numerically is in between 1D-SCF and MD methods. By reducing the number of explicit segments (pink curve), the results for R_{ce} become closer to the 1D-SCF method and deviate more from MD. This shows indeed the MC-SCF bridges between mean-field 1D-SCF and exact' MD results. It is interesting to see that relatively few explicit segments are needed to come close to the MD results.

In Fig. 5b the dependency R_{ce} is shown for the star at Θ-solvent conditions. Under theta conditions it is expected that the excluded volume effects are minor. Hence it is anticipated that the values of R_{ce} are relatively close to each other. In line with this we see a rather good agreement with the scaling prediction, $\gamma = 0.5$ for all methods, and there are small numerical differences between MC-SCF and MD results. Again the 1D-SCF underpredicts the value of R_{ce} a bit more.

In Fig. 5c the dependency R_{ce} is shown for the star at poor solvent conditions. It can be observed, apart from 1D-SCF method, all methods predict the same result, which is consistent with scaling exponent $\gamma = 0.33$.

In summary, the hybrid approach at good and theta solvent quality conditions gives results that are intermediate between those of the CG and the mean-field models. The differences in the numerical coefficients are not very large and accounting for the error bars all models show a satisfactory agreement one to another and importantly with the scaling predictions. In other words, by increasing the number of explicit segments in the MC-SCF hybrid (for sufficiently long arms) we can come closer to the exact result, but this goes at the expense of computational efficiency. When computational resources are limited we may decide to reduce the number of explicit segments and sacrifice some accuracy or *vice versa*.

3.3 Radius of gyration, R_g^2

In Fig. 6a dependencies of the radius of gyration are shown as a function of the number of monomers per arm N for the MD, the MC-SCF, and the 1D-SCF methods at the good solvent conditions. We see that all curves obey the scaling prediction of $\gamma \approx 0.588$ as well as $R_g^2 \approx N^{1.18}f^{0.41}$ (our case $f = 3$ all times) fitted experimental data.[2] Simultaneously, we compared our results with independent DPD simulations[32] (not shown). The slope of curves is consistent. The estimated error bars for MC-SCF and MD methods are mostly comparable, only for the star with $N = 200$ segments per arm, the MD data looks undersampled, whereas the MC-SCF does not change the straight line trend. Mean values of the radius of gyration R_g^2 in the MC-SCF and the 1D-SCF methods remain close to each other for all set of arm lengths. The MD results stay slightly higher with respect to other methods.

In Fig. 6b the radius of gyration dependencies are shown for Θ-solvent conditions. The data from the MD and the MC-SCF methods overlap. However, the 1D-SCF method gives slightly lower results. Moreover, the MC-SCF method with small number
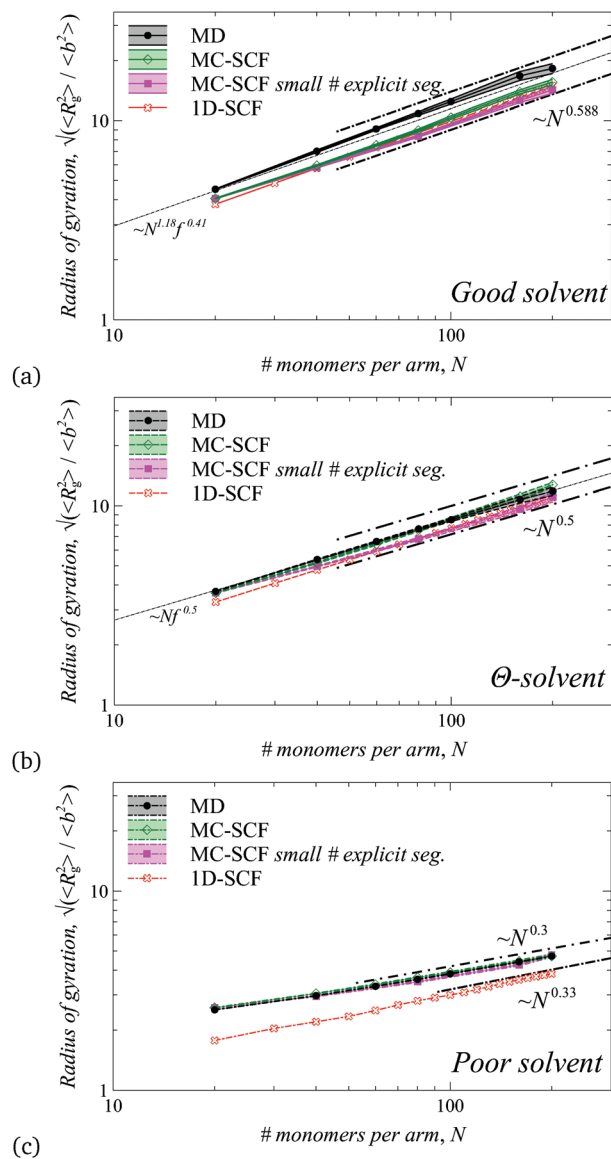
Fig. 6 $\sqrt{\langle R_g^2 \rangle / \langle b^2 \rangle}$ of the star for MD, MC-SCF and SCF methods, where $\langle b^2 \rangle$ is averaged bond length in MD and $\langle b^2 \rangle = 1$ for MC-SCF and 1D-SCF. Figure (a) Good solvent quality condition: MD parameters $\varepsilon = 1.0$, $r_{cutoff} = 2^{1/6}$, MC-SCF and 1D-SCF parameter $\chi = 0.0$. Figure (b) Θ-solvent quality condition: MD parameters $\varepsilon = 0.34$, $r_{cutoff} = 2.5$, MC-SCF and 1D-SCF parameter $\chi = 0.5$. Figure (c) Poor solvent quality conditions: MD parameters $\varepsilon = 0.7$, $r_{cutoff} = 2.5$, MC-SCF and 1D-SCF parameter $\chi = 1.5$. The number of explicit segments in the MC-SCF method could be calculated by $(fN/n) + 1$, where $f = 3$, $n = 20$. The shaded area represents the estimated error for the value.

of explicit segments gives results which represent the 1D-SCF results, as one would expect. Taking the error bars into account, all models are in good agreement with each other.

Let us now consider the dependencies R_g^2 at poor solvent condition, given in Fig. 6c. For all arm lengths we see that the results for the MD and the MC-SCF (both) methods are in good correspondence and have slightly lower scaling exponent (about $\gamma = 0.3$). The minor numerical differences between the models are similar to the ones found for theta solvent.

The 1D-SCF method shows an exponent $\gamma = 0.33$ which is the value expected from scaling theory.

3.3.1 Polymer density profile. In Fig. 7 we present the polymer density profile, that is the volume fraction φ as a function of distance from the center of the polymer star for $N = 160$ segments per arm.

The polymer density profile at good solvent is shown on the left hand side of the Fig. 7. The MD and the MC-SCF results obey the scaling prediction[33,34] $r^{-4/3}$ better than results from the 1D-SCF method. The 1D-SCF result has the strongest deviation from the scaling prediction. Simultaneously, we compared our results with independent simulations (not shown).[2,35] The slope and values were in good agreement.

The polymer density profile at Θ-solvent is depicted in the center of Fig. 7. Apart from the small distances, all methods are in good agreement one to another. The density profiles obey the scaling prediction $\varphi(r) \propto r^{-1}$ only for small distances from the center of the polymer star.[33,34]

On the right hand side of Fig. 7 the polymer density profiles are presented at poor solvent conditions. The MC-SCF (both) and the MD methods are in good mutual agreement all values of r. However, the 1D-SCF does not follow the same trend. The 1D-SCF method predicts that the star at poor solvent is collapsed to a higher density and extends less far in the solution. Clearly, the 1D-SCF underpredicts the fluctuations (in the interfacial region between the globule and the solvent) in this case.

3.3.2 Efficiency. In order to give quantitative estimation of efficiency of the MD and the MC-SCF methods, we provide estimation of integrated autocorrelation time for R_{ce} values. In Fig. 8 we present estimation of the lag τ as a function of length of the star arm N, calculated accordingly the manuscript.[36] We provide estimations for different solvent
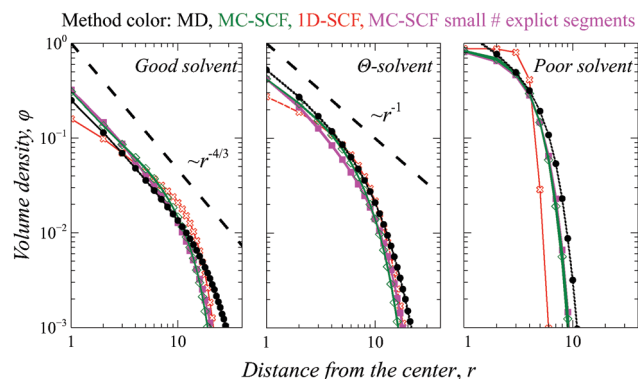
Fig. 7 The polymer density profile $\varphi(r)$ for polymer stars with $N = 160$ and $f = 3$ found by the MC-SCF (green $n = 20$, pink $n = 80$), the MD (black) and the 1D-SCF methods (red). (Left) Good solvent condition: MD parameters $\varepsilon = 1.0$, $r_{cutoff} = 2^{1/6}$, MC-SCF and 1D-SCF parameter $\chi = 0.0$. (Center) Θ-solvent condition: MD parameters $\varepsilon = 0.34$, $r_{cutoff} = 2.5$, MC-SCF and 1D-SCF parameter $\chi = 0.5$. (Right) Poor solvent condition: MD parameters $\varepsilon = 0.7$, $r_{cutoff} = 2.5$, MC-SCF and 1D-SCF parameter $\chi = 1.5$. The number of explicit segments in the MC-SCF (green curve) method is 25, for the MC-SCF method with a small number of explicit segments (pink curve) is 7. The shaded area represents the estimated error for the value.
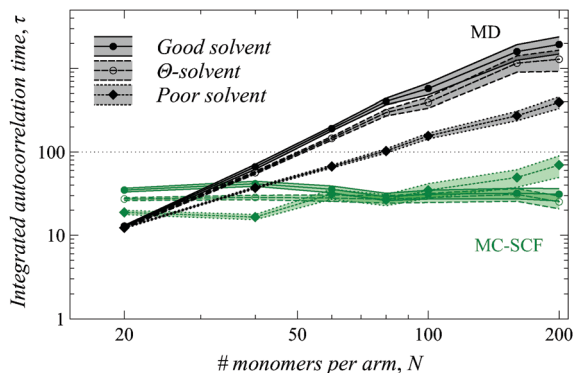
Fig. 8 The estimated integrated autocorrelation time τ as a function of number of segments per arm N. Good solvent condition: MD parameters $\varepsilon = 1.0$, $r_{cutoff} = 2^{1/6}$, MC–SCF parameter $\chi = 0.0$. Θ-Solvent condition: MD parameters $\varepsilon = 0.34$, $r_{cutoff} = 2.5$, MC–SCF parameter $\chi = 0.5$. Poor solvent condition: MD parameters $\varepsilon = 0.7$, $r_{cutoff} = 2.5$, MC–SCF parameter $\chi = 1.5$.

qualities. We can see that the MD method works more efficient for poor solvent than for other solvent conditions, whereas, the MC-SCF method gives even smaller lag for all solvent quality conditions (less than 100 MC-SCF steps).

At good and Θ solvent conditions, we can observe that with increasing segments per arm N the MD method degradates. Namely, the MD method becomes less efficient with specific MD step (our case was 150), whereas the MC-SCF slightly fluctuates around zero slope. However, we need to distinguish the MC-SCF step and the MD step. The important idea here is the time restriction for the system (24 h), which leads to the superiority of one method over another assuming machinery constrain (the same computational power).

At poor solvent condition, the MC-SCF slightly degradates at big lengths of star arms. However, the MC-SCF method still has big gap to the MD best lag.

4 Conclusions

We compared the MC-SCF method based on a combination of Monte Carlo and the SF-SCF technique with methods based on purely coarse-grained (MD) and purely mean-field models (1-gradient SF-SCF). We employed these methods on the polymer star and we focused on the size characteristics as well as the polymer density profile of a polymer star. We compared the predictive abilities of these models at different solvent quality conditions: good solvent, Θ-solvent, and poor solvent.

All models showed consistent results. The MD method (purely coarse-grained model) is the most 'exact' method that gives reliable results, however it quickly becomes computationally expensive to produce simulation results of proper statistical quality. The 1D-SCF method (purely mean-field model) is computationally less expensive in the whole range of solvent qualities. In all cases, 1-gradient SF-SCF method produced an underestimation of the properties of the system. The MC-SCF method, on the one hand, suppresses the effect of the mean-field approximation by introducing a small number of explicit (CG)

segments and, on the another hand, not as much expensive as the MD method (within the time and machinery constraints).

We focused on quantities such as the center-to-end distance R_{ce}, the radius of gyration R_g^2, and the polymer density profile $\varphi(r)$. These quantities were compared to scaling predictions[2,33,34] and typically they were in line with these. Within the statistical errors, the various methods were also consistent with each other. Only minor deviations occurred for short arm lengths.

We estimated the efficiencies of the methods by estimating the integrated autocorrelation time τ for R_{ce} values. We showed that the MD method degrades much faster than the MC-SCF with increasing number of segments per arm N. This proved that the MC-SCF method is computationally more efficient.

We found that the MC-SCF method with pivot, one-bond and one-node movements can successfully sample all solvent conditions. The relatively low number of explicitly simulated degrees of freedom in the hybrid model makes it more efficient as compared to the purely CG model (MD). Moreover, by varying the number of explicitly represented segments in the hybrid model, the MC-SCF method can be tuned to a suitable compromise between the detail of the resolution and computational cost.

Hence, our results demonstrated that the MC-SCF method is a good trade-off between the efficient 1D-SCF method and the explicit-particle representation of the MD method. In Θ-solvent condition, results of all methods are in close correspondence. In good solvent conditions, the MC-SCF method was shown to be superior to the pure 1D-SCF method. The MC-SCF method with a necessary and sufficient amount of explicit segments is numerically closer to 'exact' MD $\left(\sqrt{\langle R_{ce}^2 \rangle}, \quad \sqrt{\langle R_g^2 \rangle} \right)$, and $\varphi(r)$. At poor solvent, the MC-SCF method was superior additionally to the MD method too, in terms of generating the (uncorrelated) samples.

This overall behavior and its tunable inheritance make the MC-SCF method an interesting option for molecular modeling of macromolecular systems. The method can easily be extended to a collection of stars in a solvent, or to end-grafted chains on a surface (brush).

Conflicts of interest

There are no conflicts to declare.

Acknowledgements

References

1 G. W. Slater, C. Holm, M. V. Chubynsky, H. W. de Haan, A. Dubé, K. Grass, O. A. Hickey, C. Kingsbury, D. Sean, T. N. Shendruk and L. Zhan, *Electrophoresis*, 2009, **30**, 792–818.

2 G. S. Grest, L. J. Fetters, J. S. Huang and D. Richter, *Advances in Chemical Physics: Polymeric Systems*, 2007, vol. 94, pp. 67–163.

3 C. N. Likos, *Phys. Rep.*, 2001, **348**, 267–439.

4 Y. Zhao, S. M. Ma, B. Li, A. De Nicola, N. S. Yu and B. Dong, *Polymers*, 2019, **11**, 1–16.

5 A. De Nicola, T. Kawakatsu and G. Milano, *Macromol. Chem. Phys.*, 2013, **214**, 1940–1950.

6 J. Bergsma, J. van der Gucht and F. A. Leermakers, *Macromol. Theory Simul.*, 2019, **28**, 1–14.

7 E. Sarukhanyan, A. De Nicola, D. Roccatano, T. Kawakatsu and G. Milano, *Chem. Phys. Lett.*, 2014, **595–596**, 156–166.

8 G. J. Sevink, F. Schmid, T. Kawakatsu and G. Milano, *Soft Matter*, 2017, **13**, 1594–1623.

9 Y. L. Zhu, Z. Y. Lu, G. Milano, A. C. Shi and Z. Y. Sun, *Phys. Chem. Chem. Phys.*, 2016, **18**, 9799–9808.

10 J. Bergsma, F. A. Leermakers and J. Van Der Gucht, *Phys. Chem. Chem. Phys.*, 2015, **17**, 9001–9014.

11 B. J. Reynwar, G. Illya, V. A. Harmandaris, M. M. Müller, K. Kremer and M. Deserno, *Nature*, 2007, **447**, 461–464.

12 P. Košovan, J. Kuldová, Z. Limpouchová, K. Procházka, E. B. Zhulina and O. V. Borisov, *Soft Matter*, 2010, **6**, 1872–1874.

13 F. Weik, R. Weeber, K. Szuttor, K. Breitsprecher, J. de Graaf, M. Kuron, J. Landsgesell, H. Menke, D. Sean and C. Holm, *Eur. Phys. J.-Spec. Top.*, 2019, **227**, 1789–1816.

14 J. E. Jones, *Proc. R. Soc. A*, 1924, **106**, 463–477.

15 H. R. Warner, *Ind. Eng. Chem. Fundam.*, 1972, **11**, 379–387.

16 G. J. Fleer, M. A. C. Stuart, J. M. H. M. Scheutjens, T. Cosgrove and B. Vincent, *Polymers at Interfaces*, Springer, 1993.

17 O. V. Borisov, E. B. Zhulina, F. A. Leermakers, M. Ballauff and A. H. Müller, *Advances in Polymer Science*, Springer Berlin, Heidelberg, 2011, vol. 241, pp. 1–55.

18 O. Rud, T. Richter, O. Borisov, C. Holm and P. Košovan, *Soft Matter*, 2017, **13**, 3264–3274.

19 J. M. Scheutjens and G. J. Fleer, *J. Phys. Chem.*, 1979, **83**, 1619–1635.

20 M. Mocan, M. Kamperman and F. A. Leermakers, *Polymers*, 2018, **10**, 78.

21 F. A. M. Leermakers, J. Scheutjens and J. Lyklema, *Biophys. Chem.*, 1983, **18**, 353–360.

22 J. Bergsma, F. A. M. Leermakers, J. M. Kleijn and J. van der Gucht, *J. Chem. Theory Comput.*, 2018, **14**, 6532–6543.

23 M. Charlaganov, P. Košovan and F. A. Leermakers, *Soft Matter*, 2009, **5**, 1448–1459.

24 Z. Preisler, P. Košovan, J. Kuldová, F. Uhlík, Z. Limpouchová, K. Procházka and F. A. Leermakers, *Soft Matter*, 2011, 7, 10258–10265.

25 O. A. Evers, J. M. H. M. Scheutjens and G. J. Fleer, *Macromolecules*, 1991, **24**, 5558–5566.

26 L. D. Gelb, *J. Chem. Phys.*, 2003, **118**, 7747–7750.

27 N. Metropolis, A. W. Rosenbluth, M. N. Rosenbluth, A. H. Teller and E. Teller, *J. Chem. Phys.*, 1953, **21**, 1087–1092.

28 J. D. Weeks, D. Chandler and H. C. Andersen, *J. Chem. Phys.*, 1971, **54**, 5237–5247.

29 U. Micka, C. Holm and K. Kremer, *Langmuir*, 1999, **15**, 4033–4044.

30 R. Guida and J. Zinn-Justin, *J. Phys. A: Math. Gen.*, 1998, **31**, 8103–8121.

31 N. Clisby, *Phys. Rev. Lett.*, 2010, **104**, 1–4.

32 M. M. Nardai and G. Zifferer, *J. Chem. Phys.*, 2009, **131**, 124903.

33 M. Daoud and J. P. Cotton, *J. Phys.*, 1982, **43**, 531–538.

34 E. B. Zhulina, T. M. Birshtein and O. V. Borisov, *Eur. Phys. J. E: Soft Matter Biol. Phys.*, 2006, **20**, 243–256.

35 A. D. Cecca and J. J. Freire, *Macromolecules*, 2002, **35**, 2851–2858.

36 U. Wolff, *Comput. Phys. Commun.*, 2004, **156**, 143–153.